RESEARCH ARTICLE

Particle Design and Inhalation Delivery of Iodine for Upper Respiratory Tract Infection Therapy

Kaikai Zhang[1,2] · Xiaohong Ren[2] · Jiacai Chen[3,2] · Caifen Wang[2,4] · Siyu He[2] · Xiaojin Chen[2] · Ting Xiong[2,4] · Jiawen Su[1,2] · Shujun Wang[4] · Weifeng Zhu[1] · Jiwen Zhang[1,2,3,5] · Li Wu[1,2]

Abstract
Diseases caused by upper respiratory tract (URT) and pulmonary infections have been a serious threat to human health for millennia and lack of targeted effective therapeutic techniques. In this study, two kinds of cyclodextrin particles with typical particle shapes of nanocubes and microbars were synthesized through a facile process. Subsequently, the particles were used as carriers for loading and stabilizing iodine and characterizations were performed to demonstrate the loading mechanism. Next-generation impactor (NGI) experiments showed that iodine-loaded microbars (I_2@microbars) had a deposition rate of 79.75% in URT, while iodine-loaded nanocubes (I_2@nanocubes) were delivered to the deep lungs with a fine particle fraction (FPF) of 46.30%. Minimal inhibitory concentration (MIC) and minimal bactericidal concentration (MBC) indicated that the iodine-loaded nanocubes and microbars had similar bactericidal effect to povidone iodine solution. Cell viability studies and extracellular pro-inflammatory factor (TNF-α, IL-1β, IL-6) evaluations demonstrate noncytotoxic effects of the blank carriers and anti-inflammatory effects of iodine-loaded samples. The irritation of the rat pharynx by I_2@microbars was evaluated for the behavioral observations, body weight changes, histopathological studies, and TNF-α, IL-1β, and IL-6 levels in pharyngeal tissues. The results showed that I_2@microbars had no irritation to rat pharyngeal tissues at therapeutic doses. In conclusion, the present study provides novel treatment of URT infections via supramolecular cyclodextrin carriers for URT local therapy with iodine loading by a solvent-free method, which enhances the stability and reduces the inherent irritation without inhibiting their antimicrobial effects.

KEY WORDS upper respiratory tract infection · inhalation · drug carrier · iodine · gas–solid reaction

Kaikai Zhanga, Xiaohong Renb and Jiacai Chenc are co-first authors.

✉ Weifeng Zhu
zwf0322@126.com

✉ Jiwen Zhang
jwzhang@simm.ac.cn

✉ Li Wu
wuli@simm.ac.cn

1 Key Laboratory of Modern Preparation of TCM, Ministry of Education, Jiangxi University of Chinese Medicine, No. 16 88, Meiling Road, Nanchang 330004, China

2 Center for Drug Delivery Systems, Shanghai Institute of Materia Medica, Chinese Academy of Sciences, No. 501, Haike Road, Shanghai 201210, China

3 Nanjing University of Chinese Medicine, No. 138, Xianlin Road, Nanjing 210000, China

4 College of Pharmacy, Shenyang Pharmaceutical University, No. 103, Wenhua Road, Shenyang 110016, China

5 NMPA Key Laboratory for Quality Research and Evaluation of Pharmaceutical Excipients, National Institutes for Food and Drug Control, Beijing 100050, China

INTRODUCTION

Respiratory infection is one of the common respiratory diseases, which seriously affects health-related quality of life (1). Since the upper respiratory tract (URT) is the gatekeeper of the respiratory microbiota, the proximity of URT to the external environment allows adherence and colonization of diverse and abundant microbiota. URT infections mainly include rhinitis, pharyngitis, tonsillitis, and otitis media, accounting for about 87.5% of the total number of respiratory infections (2, 3). The common respiratory pathogen in infected patients was caused by viruses, bacteria, mycoplasma, or chlamydia (4, 5). Additionally, the decline in physical function and immunity of the elderly increases the incidence of URT infections. Although most URT infections are self-limited, life-threatening complications occasionally occur, and its multiplicity also causes a huge medical burden (6, 7). Nowadays, the COVID-19 epidemic that develops serious respiratory tract problem is still rampant all over the world. How to reduce the risk of virus infection in patients

with respiratory infections has attracted the attention of health organizations. Antibiotic drugs including cephalosporins, macrolides, and quinolones are usually orally or intravenously administered for the treatment of acute and severe URT infections in clinical practice. However, the overuse of antibiotics caused by these practices is a contributing factor to the development of drug resistance. According to recent surveys, up to 50% of antibiotics are abused in the world every year due to inadequate regulation (8, 9). The systemic administration route could cause adverse reactions to other tissues while delivering drugs to the lesion. Even worse, the emergence of resistance cannot be completely eliminated even by topical administration, such as inhaled antibiotics (10). In addition, not only does the drug resistance caused by misuse leads to a crisis in the use of antibiotics, but also the emergence of various "super drug-resistant bacteria" poses a more serious threat to human health (11). Therefore, it is particularly significant to design non-antibiotic anti-infective drugs for local delivery of URT.

The formulations for treatment of URT disease included lozenges (12, 13), buccal tablets, sprays (14, 15), and traditional Chinese medicines. The lack of research on URT topical therapeutic formulations has greatly limited the progress in the treatment of URT disease. Nevertheless, lozenges and buccal tablets are at risk of irritating the digestive tract with primary dose absorbed via gastric-intestinal tract. Sprays are limited due to weak portability, high cost, and susceptibility to spoilage. The traditional Chinese medicines are not delivered via inhalation for the therapy of URT diseases. Recently, dry powder inhalers (DPIs) have attracted more and more attention because they can deliver active pharmaceutical ingredients (API) non-invasively to the deep respiratory tract for achieving curative effect (16–20). Besides, among the available inhalation formulations, DPIs have become preferred for their advantages over other inhalation formulations, e.g., low cost, environmental friendly, high portability, good stability, and processability. The particle size and shape were extremely important factors to the behaviors of DPI in the respiratory tract (21, 22). To effectively deliver particles into the lung, the aerodynamic particle size must be within a suitable range of 1–5 μm. In addition, particles with aerodynamic particle size smaller than 3 μm are believed to be more suitable for alveolar drug delivery, whereas particles of 3–5 μm are expected to be deposited more in the middle of the bronchial tree and in the upper airways (23). Accordingly, it is very meaningful to apply DPI's morphology and particle size control technology to design a suitable carrier for highly URT deposition, thereby paving the way for the treatment of URT diseases.

Iodine, an inorganic substance, has been extensively studied and used for more than a century since its discovery (24). Due to its broad spectrum (activity against aerobic and anaerobic bacteria as well as viruses, chlamydia, and fungi)

and low price, it is widely used for disinfection and sterilization both *in vivo* and *in vitro*. Despite a long history of effective usage, iodine has not shown significant resistance (25). Currently, the most frequently used iodine preparations are tincture of iodine and povidone iodine (PVP-I). Tincture of iodine, prepared by dissolving iodine monomers and potassium iodide in ethanol, is a topical skin infection and disinfectant (26), which stains easily, irritates highly, and requires deiodination after use. PVP-I is a complex of polyvinylpyrrolidone and iodine monomers, with an effective iodine content of about 10%. Notably, iodine preparations, such as povidone iodine spray for topical usage, and cydiodine buccal tablets are often used in the treatment of URT diseases (27).

The application of cyclodextrin (CD) as a carrier for drug loading has been long-standing, and a large number of studies have shown that drugs encapsulated by CD exhibit advantages such as reduced irritation (28), enhanced water solubility (29), increased stability (30), and improved bioavailability (31). Therefore, selecting a suitable CD carrier to reduce the irritation and improve solubility of the drug is a reliable option. While respiratory drug delivery requires rapid drug dissolution in the drug delivery area after inhalation, the solubilities of β-CD (18 mg/mL) and α-CD (140 mg/mL) are relatively low; thus, γ-CD with higher solubility (240 mg/mL) is the preferred choice for respiratory drug delivery. Furthermore, β-CD tends to bind to cholesterol in plasma to form insoluble particles (32); while γ-CD could be of injectable grade, it is generally regarded as safe to be used as inhalation.

In this study, gamma-cyclodextrin (γ-CD)–based carriers with different size and morphology were designed by an optimized controlled crystallization method. In addition, gas–solid reaction technology was applied to load iodine into the molecular cavities of the particles. A proof of concept design was validated by aerodynamic deposition and other characterizations for the treatment of URT infections.

MATERIALS AND METHODS

Materials

The γ-CD was purchased from Maxdragon Biochem Co., Ltd (Guangdong, China). Pharmaceutical grade crystalline iodine (I₂) was provided by Shandong Jiejing Pharmaceutical Co., Ltd (China). Yeast extract and tryptone were purchased from Thermo Fisher Scientific Ltd (USA). Isopropanol and methanol of HPLC grade were procured from J&K Scientific Ltd (Shanghai, China). Bicinchoninic acid (BCA) assay was provided by Cloud-Clone Co., Ltd (Wuhan, China). ELISA for TNF-α, IL-1β, IL-6, potassium iodide (KI), agarose, and other reagents of analytical grade were all obtained from Sinopharm Chemical Reagent Co., Ltd (Shanghai, China).

Lipopolysaccharide (LPS, L2630-10MG) was purchased from Sigma-Aldrich (St. Louis, MO, USA). Water was purified by passing through a reverse osmosis unit of a Milli-Q water system (Millipore, France).

Preparation of Nanocubes and Microbars of γ-CD

The syntheses of nanocubes and microbars were based on the previous reports with slight adjustments (33). γ-CD (4.50 g) and KI (0.518 g) were dissolved in 20 mL of deionized water and filtered using a 0.45 μm syringe filter. The above filtrate was stirred for 5 h at 50 °C and then dropped into vigorously stirred isopropanol (125 mL, 1500 r/min) at room temperature. The white emulsion was centrifuged (4000 r/min, 5 min) and the precipitate was washed once with ethanol (125 mL) to obtain nanocubes or once with isopropanol (125 mL) to obtain microbars. Ultimately, the precipitate was collected and dried in the oven at 60 °C for 12 h.

Loading of I_2 into Nanocubes and Microbars

Gas–solid reaction was used for the loading of iodine in this research. Previous investigation on the effects of reaction temperature (45 °C, 60 °C, 75 °C) and duration (0.5 h, 1 h, 2 h) on iodine loading efficiency showed that the optimal loading temperature was 60 °C and the ideal duration was 1 h. Briefly, dried nanocube or microbar powders (2.50 g) were precisely weighed into EP tubes; 0.132 g, 0.278 g, 0.625 g, and 1.071 g of iodine were added to prepare I_2 samples (I_2@nanocubes, I_2@microbars) containing 5%, 10%, 20% and 30% iodine; e.g., EP tubes were capped, sealed and put in an oven at 60 °C for 1 h.

Quantification of I_2 Loaded in Nanocubes and Microbars

The contents of iodine were detected by potentiometric titration. Briefly, samples were weighed precisely (20 mg) in the titration cup and dissolved with 40 mL potassium iodide aqueous solution (0.25 mol/L). Next, the solution was titrated using sodium thiosulfate standard titrant (0.005 mmol/L) by the automatic potentiometric titrator (ZDJ-4B, China). The effective iodine content in the sample was calculated according to the formula mentioned in the article (34).

Characterization

Scanning Electron Microscopy (SEM)

The morphologies of nanocubes, I_2@nanocubes, microbars, and I_2@microbars were determined by SEM (SU7000, Hitachi). Samples were sprinkled on the conductive glue and coated with gold before observation.

Thermogravimetric Analysis (TGA)

Thermogravimetric analyzer (Perkin-Elmer Pyris, USA) was used for thermogravimetric analysis (TGA) of iodine, γ-CD, nanocubes, I_2@nanocubes, microbars, and I_2@microbars with a heating rate of 20 °C/min under nitrogen flow rate of 20 mL/min. The weight losses of the samples were measured over the temperature range from 25 to 600 °C.

Differential Scanning Calorimetry (DSC)

The DSC curves of iodine, γ-CD, nanocubes, I_2@nanocubes, microbars, and I_2@microbars were measured with differential scanning calorimeter (PerkinElmer DSC 8500, USA) in the temperature range from 25 to 300 °C, at heating rate of 10 °C/min, with nitrogen flow rate of 30 mL/min.

Synchrotron Radiation-Fourier Transform Infrared Spectroscopy (SR-FTIR)

SR-FTIR spectra of iodine, γ-CD, nanocubes, I_2@nanocubes, microbars, and I_2@microbars were collected using a spectrometer (Nicolet 6700, Thermo Scientific, USA), which was obtained in Shanghai Synchrotron Radiation Facility (SSRF). Samples were mixed with KBr and compressed in a hydraulic press to thin tablets. Each tablet was recorded with 64 scans in a wavenumber range of 400–4000 cm^{-1} at a resolution of 4 cm^{-1}.

Powder X-ray Diffractometry

Powder X-ray diffractometry (PXRD) of iodine, γ-CD, nanocubes, I_2@nanocubes, microbars, and I_2@microbars were performed to measure the crystallinity of the powders. Diffractograms were collected with a Bruker D8 Advance diffractometer (Bruker, Germany). Powders were irradiated with monochromatized CuKα radiation ($\lambda = 1.54$ Å) and inspected at a tube voltage of 40 kV and current of 40 mA at a scan speed of 0.1 s/step in a 2θ angle range of 3–40°.

Evaluation of Powder Flowability

Hausner ratio and Carr index were measured to characterize the flow properties of the powders based on the measurement of the tapped density and bulk density of dry powders. An appropriate amount of powder was placed in a 10 mL graduated cylinder until 9 ± 1 mL for its volume. The initial volume V_0 was read, and the final volume V_f was recorded by tapping the cylinder until the volume of the powder no longer changed. The mass of dry powder added was noted as m_0. The bulk density (ρ_b) and the vibrational density (ρ_t) were calculated by Eq. 1 and Eq. 2, respectively. Hausner ratio (HR) and Carr index (CI) were calculated according to Eq. 3 and Eq. 4, respectively.

$$\rho_b = m_0/v_0 \tag{1}$$

$$\rho_t = m_0/v_f \tag{2}$$

$$HR = \rho_t/\rho_b \tag{3}$$

$$CI(\%) = \frac{\rho_t - \rho_b}{\rho_t} \times 100 \tag{4}$$

In Vitro Aerosol Dispersion Performance

The aerodynamic size is one of the critical factors affecting the deposition efficiency of inhaled particles. As a rule, particles of aerodynamic size 1–5 µm are served as the primary component of pulmonary inhalation formulations. NGI (NGI-094, Copley Scientific Ltd., Nottingham, UK) was used as a routine method determining the aerodynamic size and deposition efficiency *in vitro* of drug particles. The NGI experimental conditions were set according to the United States Pharmacopeia (USP 35) Chapter < 601 > and relevant literature (35). Emptying rate as an important indicator for evaluating DPIs was also tested. In this study, NGI was used to determine the deposition efficiency and emptying rate between two different carriers in URT. Firstly, shells of empty capsules were precisely weighed (W_1), filled each capsule with nanocube or microbar powders 20 mg, and accurately weighed respectively (W_2). Adjust the flow-control valve of critical flow controller (TPK 100i) until the pressure drop across the inhaler was 4.0 kPa (the pressure drops when the lungs inhale). Then, the flow rate (Q_{out}) was measured (inhaler: RS01-M, Plastiape Spa). Aerosols were produced with a run time of 3.7 s ($T = 240/Q_{out}$) and an air flow rate of 65 L/min (the actual average flow rate measured in the experiment). Five capsules were taken at a time, and measurements were repeated for 3 times. The capsule weight was measured after emptying (W_3), and the emptying rate was calculated as shown in Eq. 5. All parts were washed with solvent (methanol:water = 10:90, v/v) and the samples were taken for HPLC.

Quantitation of γ-CD was performed by HPLC-RID (Agilent 1260, Agilent Technologies). The Inert Sustain AQ-C18 column (250 mm × 4.6 mm, 5 µm) was used for separation with column temperature at 30 ℃. The mobile phase was consisted of methanol and water (10:90, v/v) and eluted at the flow rate of 1.0 mL/min with 50 µL of injection volume. Finally, the deposition ratio, fine particle fraction (FPF, Eq. 6), and median mass aerodynamic diameter (MMAD) of the particles were calculated by using CITDAS 6.01 (Copley scientific, Inc., Nottingham, UK) to investigate the inhalability of

medicinal particles. The deposition rate in URT (adaptor, throat, preseparator stage 1) was calculated by Eq. 7.

$$Emptying\ rate\ (\%) = \frac{(W_2 - W_3)}{(W_2 - W_1)} \times 100 \tag{5}$$

$$FPF(\%) = \frac{FPD}{ED} \times 100 \tag{6}$$

$$Upper\ airway\ deposition\ rate\ (\%) = \frac{Adaptor + Throat + Preseparator + Stage\ 1}{ED} \times 100 \tag{7}$$

Antimicrobial Activity Against *S. aureus* and *E. coli*

The antibacterial activities of the iodine-loaded nanocubes and microbars were evaluated by the microplate microdilution method. Activated *S. aureus* CMCC (B) 26,112 and *E. coli* CMCC (B) 44,102 were cultured into LB nutrient medium and incubated at 37 °C for 6 h on a shaker at 200 rpm. Then, fresh *S. aureus* and *E. coli* were regulated to 1×10^6 CFU/mL by turbidimetry. Potassium iodide was selected as a co-solvent with a concentration of 0.25 mol/L so as to prepare the samples into homogeneous solutions for a reasonable assessment of antimicrobial activity. I_2@nanocubes, I_2@microbars, and PVP-I (5%) were prepared as solutions containing 3 mg/mL or 2 mg/mL of iodine, while the blank carriers' concentration was the same as the carriers' concentration contained in the corresponding iodine-loaded samples. Next, solutions were serially diluted to 10 consecutive concentrations and added to a 96-well plate (50 µL/well), with wells 1–10 being the serial concentrations of the samples. As control, 50 µL PBS, 50 µL and 100 µL KI solution were added to wells 11, 12 and 13, respectively. Then, 50 µL of bacterial suspension diluted to 1×10^6 CFU/mL was added into wells 1–12, which was to verify that PBS or KI solution would not have an effect on the growth and reproduction of bacteria. And the purpose of not adding bacterial solution in well 13 was to verify that the blank solution would not stain with miscellaneous bacteria during the whole antibacterial experiment, and to ensure the reliability of the experimental results. All the above wells were triplicated in parallel in 3 rows. Then, PBS was added to the peripheral wells of the microplates to ensure stable humidity levels. After that, the 96-well plate was slightly shaken to make the mixture uniform. Minimum inhibitory concentration (MIC) values were recorded and calculated after 18 h incubation at 37 °C. After the MIC determination of the samples, aliquots of 50 µL from each well which showed no visible bacterial growth were streaked onto LB agar plates and incubated at 37 °C for 24 h. The minimum bactericidal concentration (MBC) was the lowest

concentration showing no colonies on the LB agar. All the experiments were carried out in triplicate.

Cytotoxicity Analysis and Extracellular Pro-inflammatory Factors (TNF-α, IL-1β, IL-6) Assay

Cell Counting Kit-8 (CCK-8) was used to investigate the cytotoxicity of the iodine-loaded samples. Briefly, MHS (alveolar macrophages) or A549 cells (human lung alveolar carcinoma epithelial cells) were seeded into 96-well plates and maintained in a humidified incubator with 95% air and 5% CO_2 at 37 °C. After being incubated overnight, a series of samples (200 µL, molecular iodine concentration of I_2@ nanocubes or I_2@microbars: 0.78–12.50 µg/mL, concentration of nanocubes or microbars: 15.62–250 µg/mL) was added to the medium and incubated for 24 h. Then, CCK-8 solution (15 µL) was added to each well and incubated for 2–4 h, and the absorbance was measured at 450 nm using a microplate reader (Multiskan GO, Thermo Fisher). Cell viability (%) was calculated as Eq. 8.

$$\text{Cell viability (\%)} = \frac{\left(A_{\text{sample}} - A_{\text{blank}}\right)}{\left(A_{\text{control}} - A_{\text{blank}}\right)} \times 100 \qquad (8)$$

Extracellular pro-inflammatory factors (TNF-α, IL-1β, IL-6) were determined using ELISA kits following the manufacturer's instructions. Briefly, MHS cells were pre-treated with 5 µg/mL LPS for 2 h and then incubated with iodine-loaded carriers at different concentrations at 37 °C for 12 h. The culture mediums after incubations (100 µL) were obtained and transferred to the ELISA plate. After incubations at 25 °C for 2 h, each well was washed with washing buffer. Then, the mouse conjugate (100 µL) was added to each well for 2 h at room temperature. After washing carefully, the plate was finally incubated with substrate solution (100 µL) for 30 min at room temperature and blocked by adding stop reagents. The absorbance was detected by a microplate reader (Multiskan GO, Thermo Fisher) at 450 nm wavelength.

Irritation of Pharyngeal Mucosa with I₂@microbars

Animals

Eighteen healthy male Sprague Dawley rats, weighing 200 ± 20 g (provided by Beijing HFK Bioscience Co. Ltd.), were used for this study. All rats were acclimatized under standard hygiene conditions for 7 days before the experiments at a controlled temperature of 25 ± 1 °C, humidity of $50 \pm 10\%$, and a 12 h light/dark cycle. All animal experiments were performed in compliance with the Institutional

Animal Care and Use Committee of Shanghai Institute of Materia Medica, Chinese Academy of Sciences (IACUC Application No. 2021–06-ZJW-35).

Experimental Design

Eighteen rats were randomly divided into 3 groups: normal control group, low-dose group (0.4 mg/kg), and high-dose group (0.8 mg/kg). The dose administered to rats was calculated based on the clinically used dosage (64 µg/kg) of cydiodine buccal tablets. The rats were weighed and observed for normal pharyngeal area and feeding behavior during experiment. After the administration group was anesthetized with isoflurane inhalation and immobilized, the rats' tongues were gently pulled out to expose the pharynx and the drug powder (0.25% specification I_2@microbars) was sprayed onto the pharynx area once a day for 7 consecutive days. The normal control group was subjected to the same experimental operation except without administered. It should be noted that all rats were fasted from food and water for 30 min after each administration. After 12 h of drug administration on day 7, the rats were fasted for 12 h and sacrificed. The pharyngeal tissues were taken and followed by washing with sterile saline to remove blood and mucus. The pharyngeal tissues of three randomly selected rats in each group were fixed in neutral paraformaldehyde to prepare paraffin sections. Then, the mucosal morphology was observed under light microscopy after H&E staining. The other samples were placed at − 80 °C for the detection of inflammatory factors.

RESULTS AND DISCUSSION

Morphology and Particle Size

The nanocubes and microbars of γ-CD are displayed in Fig. 1. The morphology of ethanol wash group presented regular cubic shape with a side length of 200–600 nm. The isopropanol wash sample exhibited bar shape and distributed in the range of 1–5 µm. The pictures showed that the morphology and size stayed no obvious change when iodine was loaded. It meant that this solvent-free drug loading method did not change the physical morphology of the two kinds of drug carriers.

Iodine Loading Efficiency

In the range of iodine material ratio of 5–20%, the drug loading efficiencies of two carriers were similar, with both above 90% (Table I). This indicated that the two carriers

could achieve efficient loading of iodine under solvent-free and mild conditions. When the material ratio was 30%, the drug loading of nanocubes and microbars was 24.61% and 27.28%, respectively (Fig. 2), with significant differences between them, suggesting that the two carriers have different affinities for iodine. It should be noted that with the increase of the proportion of iodine materials, the carriers gradually saturated with iodine capture, and the uncaptured iodine mainly attached to the vessel walls.

Powder Flowability

The flowability of the powder is naturally a key factor in achieving effective respiratory deposition of DPI formulations. In addition, good flow properties ensure the accuracy of dose and hence allow the fluidization and release of powders from the drug delivery devices (36). The Hausner ratio (HR) and Carr index (CI) were widely used to characterize the flowability of powders as the key indicators for powder flowability evaluation. Generally, powders with HR between 1.12 and 1.18 and CI values between 11% and 15% were recognized as a good flowability (37). Table II illustrates that the Hausner ratio and Carr index of microbars

and nanocubes did not change significantly before and after iodine loading. Additionally, all four samples tested showed poor flowability according to HR and CI values. On the one hand, the poor mobility of microbars may lie in the rod-like morphology of the particles, which easily lead to bridging. On the other hand, nanocube particles possessed small diameter and a large specific surface area, resulting in high friction.

Upper Respiratory Tract and Lung Deposition

Although the flowability of the four powder samples was not high indicated by Hausner ratio and Carr index, the NGI experiments showed that all four dry powders were able to be emitted smoothly when tested in capsules, with an average emptying rate of over 98%. This indicated that the properties of respirable particles cannot be evaluated by conventional flowability alone and that aerodynamic performance may be more reliable. Figure 3 shows the deposition profiles of microbars, nanocubes, I_2@microbars, and I_2@nanocubes on each stage of NGI. The results of NGI experiments showed significant differences in the distribution of the two forms of carriers in the respiratory tract (Table III). Among them, the depositions in URT (adaptor, throat, preseparator, stage
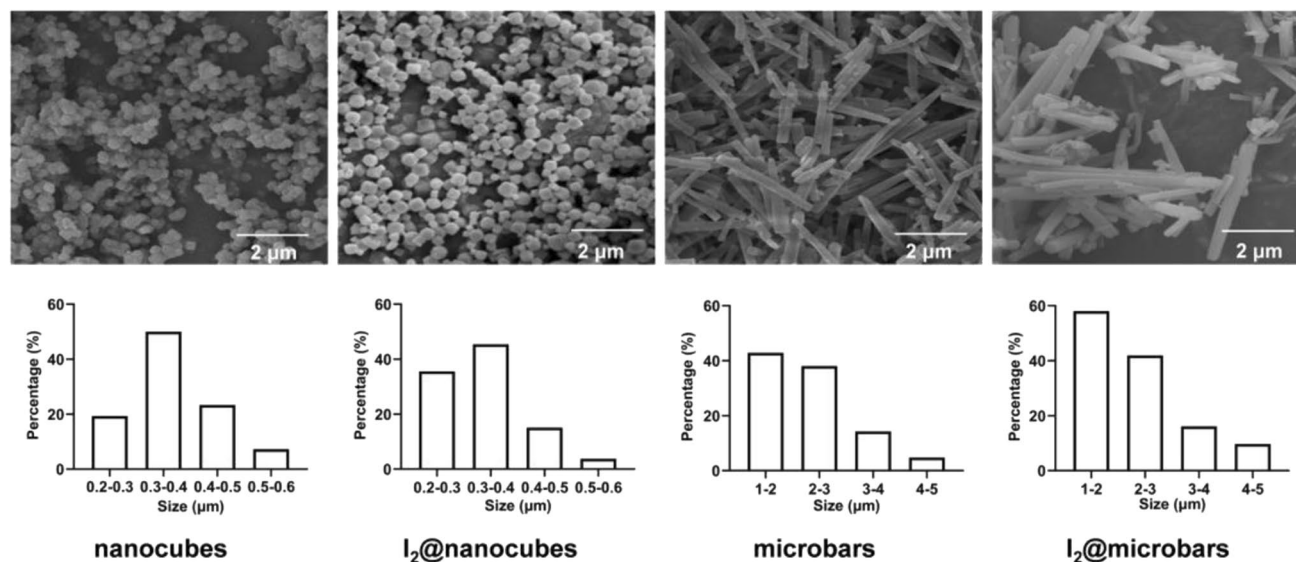

Fig. 1 SEM images and particle size distributions of nanocubes, I_2@nanocubes, microbars and I_2@microbars

Table I Iodine Loading and Efficiency of Two Carriers (Mean ± SD, $n=3$)

Material ratios (%)	Nanocubes		Microbars	
	Iodine loading (%)	Efficiency (%)	Iodine loading (%)	Efficiency (%)
5	4.84 ± 0.04	96.78 ± 0.73	4.77 ± 0.01	95.31 ± 0.11
10	9.21 ± 0.05	92.12 ± 0.45	9.62 ± 0.11	96.16 ± 1.13
20	18.39 ± 0.18	91.96 ± 0.90	19.09 ± 0.02	95.43 ± 0.09
30	24.61 ± 0.24	82.04 ± 0.80	27.28 ± 0.37	90.94 ± 1.24
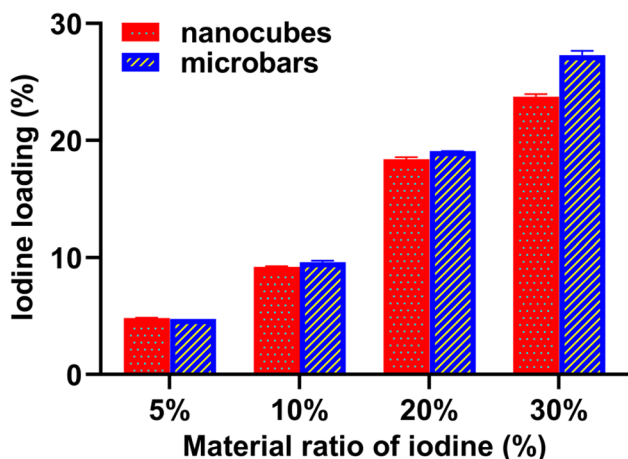
Fig. 2 Drug loading of two carriers in the material ratio range of 5–30% (mean $\pm$ SD, $n = 3$)

respectively. The above results suggested that even nanocubes had significant advantages for pulmonary delivery, while the rod-shaped vector facilitated drug delivery to the URT. In addition, the NGI distribution of two samples loaded with iodine showed no significance with the blank vector. For example, the deposition rate of I_2@microbars in the URT was nearly 80%, and I_2@nanocubes had a FPF of 46.30%, implying that different vectors have specific potential for targeted drug delivery to specific parts of the respiratory tract. The microbars facilitated drug delivery to the URT, while the nanocubes have significant advantages for pulmonary delivery. In addition, the NGI distributions of the iodine-loaded samples were not significantly different from those of the blank vectors, indicating both vectors have great potential for targeted drug delivery to different parts of the respiratory tract and the shape of KI-conjugated CD particles controls the particle distribution in URT.

Characterizations for Iodine Loading Mechanism

Figure 4a is the SR-FTIR spectra of iodine molecules, γ-CD, nanocubes, microbars, I_2@nanocubes, and I_2@microbars.

1) were significantly different. The deposition rate of microbars in the upper airway was $79.27 \pm 0.47\%$, while nanocube particles were $43.18 \pm 4.06\%$. The FPF values of microbars and nanocubes were $16.41 \pm 1.47\%$ and $51.65 \pm 4.28\%$,

Table II Flowability Parameters of Powders (Mean $\pm$ SD, $n = 3$)

Samples	Bulk density (g/mL)	Tapped density (g/mL)	Hausner ratio	Carr index (%)
Nanocubes	0.19 ± 0.01	0.35 ± 0.01	1.86 ± 0.05	46.15 ± 1.47
I_2@nanocubes	0.19 ± 0.00	0.34 ± 0.01	1.83 ± 0.06	45.26 ± 1.78
Microbars	0.15 ± 0.00	0.29 ± 0.01	1.95 ± 0.07	48.63 ± 1.92
I_2@microbars	0.15 ± 0.00	0.30 ± 0.01	1.96 ± 0.04	49.02 ± 1.00

I_2@*nanocubes*, iodine-loaded nanocubes; I_2@*microbars*, iodine-loaded microbars.

Fig. 3 Aerodynamic deposition performance of nanocubes, microbars, I_2@nanocubes, and I_2@microbars tested by next-generation impactor and the deposition fraction in the upper respiratory tract and lungs (mean $\pm$ SD, $n = 3$)
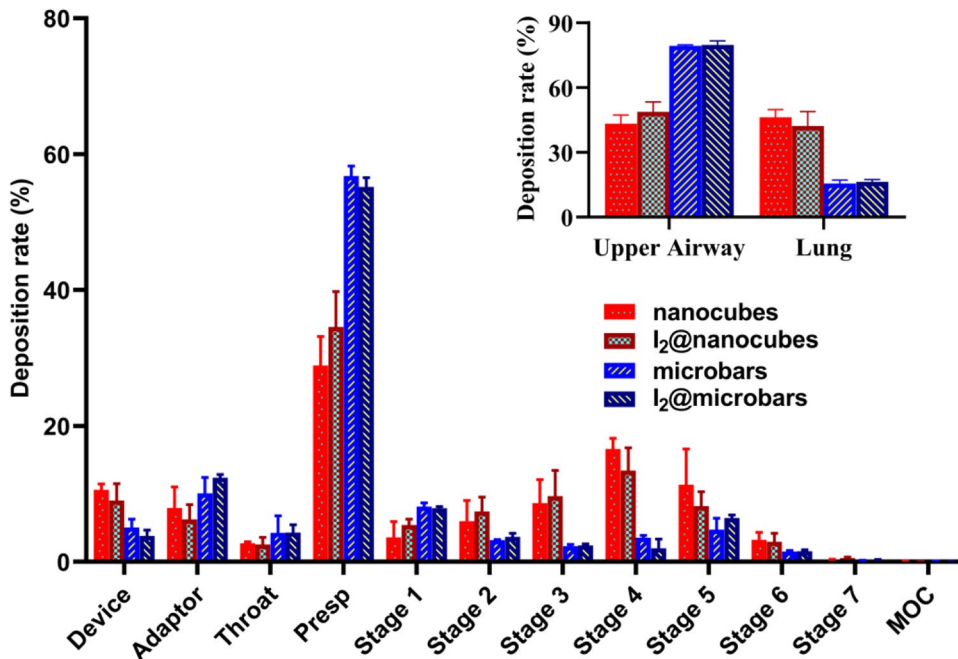
Among them, the characteristic absorption peak of iodine molecule was at 1400.31 cm^{-1}. The spectrum revealed the existence of -OH (3383.35–3389.18 cm^{-1}) group, this peak was wide, and there was no significant change before and after iodine loading. 2926–2932 cm^{-1} was the -CH$_2$- stretching vibration peak. 1156–1157 cm^{-1} was the asymmetric stretching vibration peak of C–O–C. 1025–1027 cm^{-1} was the C-O stretching vibration peak. The above data suggested that the iodine molecule was loaded into the cavities of γ-CD.

The PXRD (Fig. 4b) of I$_2$@nanocubes and I$_2$@microbars showed no characteristic peaks of either iodine or the carries. This might be attributed to the crystal defects due to the position of iodine in the unit cell, in which I$_2$ combined with I$^-$ and irregularly distributed in the frameworks weakening the diffraction peaks. The order of crystals also changed

Table III Aerodynamic Parameters of Two Carriers and the Iodine-Loaded Particles (Mean ± SD, $n=3$)

Parameters	Nanocubes	I$_2$@nano-cubes	Microbars	I$_2$@micro-bars
MMAD (μm)	2.26 ± 0.59	2.54 ± 0.33	3.89 ± 0.82	3.84 ± 0.54
GSD	2.10 ± 0.14	2.48 ± 0.24	3.16 ± 0.51	3.38 ± 0.54
FPF (%)	51.65 ± 4.28	46.30 ± 6.07	16.41 ± 1.47	17.03 ± 1.23

I$_2$@nanocubes, iodine-loaded nanocubes; *I$_2$@microbars*, iodine-loaded microbars; *MMAD*, median mass aerodynamic diameter; *GSD*, geometric standard deviation; *FPF*, fine particle fraction.

due to the strong interaction between the carries and I$_2$. It further indicated that iodine was loaded into γ-CD cavities and that this interaction changed the physical properties of the two carriers.

From the analysis of the DSC pattern (Fig. 4c), the molecule iodine had an exothermic peak at 125 ℃ and a thermal absorption peak at 114 ℃ and 185 ℃, which corresponded to the melting and boiling points of iodine, respectively. However, there was no obvious heat absorption or exothermic peak for γ-CD in the range of 25–300 ℃. Interestingly, nanocubes and microbars showed thermal behaviors between 265 and 285 ℃, which were inconsistent with γ-CD. Meanwhile, nanocubes and microbars did not show the characteristic peaks of iodine molecules in the DSC patterns after iodine loading and were not consistent with their thermal behaviors before iodine loading, suggesting that iodine molecules have entered and interacted with their cavities. The disappearance of the peaks of I$_2$@microbars and I$_2$@nanocubes may be caused by the interaction of molecular iodine with the carriers, which further validated the PXRD results.

From Fig. 4d, it can be observed that the weight loss of iodine was 0.75% at 25–45 ℃, and the sharp weight loss of 99.25% at 45–133 ℃ was due to the thermal sublimation of iodine molecules. Nanocubes and microbars possessed a highly similar thermal behavior according to the curves. In addition, the weight loss of I$_2$@nanocubes and I$_2$@microbars at 25–180 ℃ was basically the same as that of nanocubes and microbars. However, in the range of 180–280 ℃, the weight

Fig. 4 Characterizations of I$_2$, γ-CD, nanocubes, microbars, I$_2$@nanocubes, and I$_2$@microbars. **a** SR-FTIR spectra. **b** PXRD patterns. **c** DSC thermograms. **d** TGA thermograms
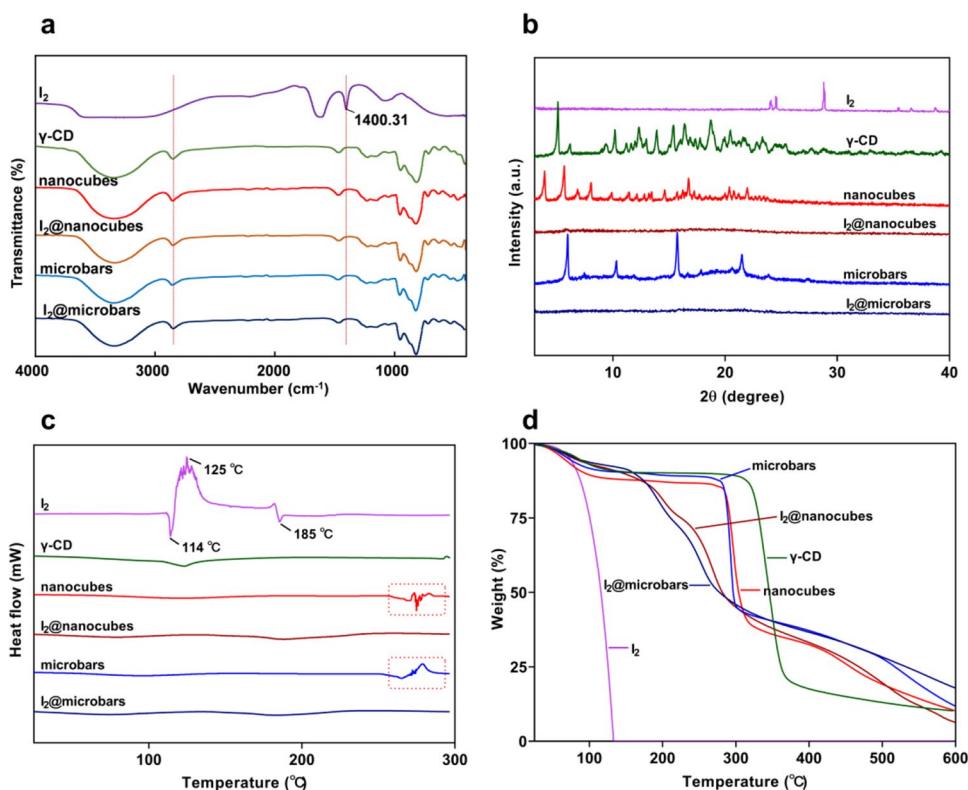
Table IV MIC and MBC of Each Sample Against *E. coli* and *S. aureus*

| Samples	*E. coli*		*S. aureus*	
	MIC (µg/mL)	MBC (µg/mL)	MIC (µg/mL)	MBC (µg/mL)
I$_2$@nanocubes	500	500	93.75	250
I$_2$@microbars	500	500	93.75	250
PVP-I	500	500	93.75	250

MIC, minimal inhibitory concentration; MBC, minimal bactericidal concentration; I$_2$@nanocubes, iodine-loaded nanocubes; I$_2$@microbars, iodine-loaded microbars; PVP-I, povidone iodine.

losses were 35.80% and 36.67%, respectively, distinct from blank carriers. These phenomena indicated that iodine molecules were highly dispersed in the cavities of γ-CD carriers and the thermal stability was significantly improved.

Antibacterial Activity

Experiments were carried out to verify whether iodine exhibited good antibacterial activity after inclusion by cyclodextrin. The antibacterial activities of I$_2$@nanocubes, I$_2$@microbars, PVP-I, and two blank carriers were measured by determining the minimum inhibitory concentration

(MIC) and minimum bactericidal concentration (MBC) against *E. coli* and *S. aureus*. The MIC and MBC values of each group of samples against standard strains of *E. coli* and *S. aureus* are presented in Table IV. Both blank vectors did not show inhibition against *E. coli* and *S. aureus* in the concentration range of 0.035–27 mg/mL and therefore were not listed in the table. The MIC and MBC of I$_2$@nanocubes and I$_2$@microbars against *E. coli* were both 500 µg/mL, which were the same as those of PVP-I. In addition, for *S. aureus*, all groups of iodine-containing samples showed superior bactericidal effects compared to *E. coli* in terms of MIC and MBC results. Briefly, the MIC of the two
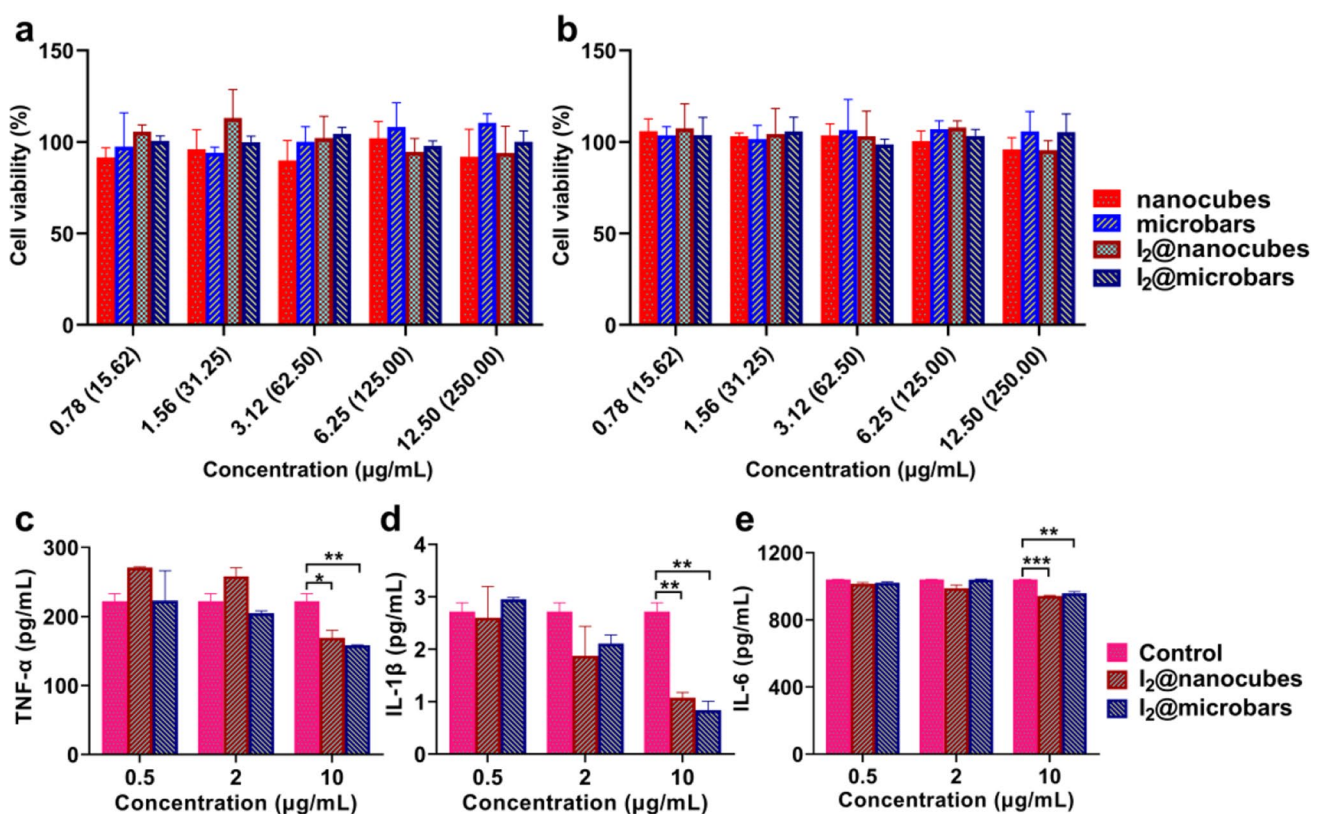
Fig. 5 Cytotoxicity and anti-inflammatory effect study. **a** MHS cell viability and *in vitro* cytotoxicity of blank carries, I$_2$@nanocubes, and I$_2$@microbars, **b** A549 cell viability and *in vitro* cytotoxicity of blank carries, I$_2$@nanocubes, and I$_2$@microbars (molecular iodine concentration of I$_2$@nanocubes or I$_2$@microbars: 0.78–12.50 µg/mL, con-centration of nanocubes or microbars: 15.62–250 µg/mL). Levels of TNF-α (**c**), IL-1β (**d**), and IL-6 (**e**) in LPS-stimulated MHS cells after incubation with iodine-loaded samples ($n = 6$, *$P < 0.05$, **$P < 0.01$, ***$P < 0.001$)

iodine-loaded samples against *S. aureus* was nearly 1/6 of that against *E. coli*, and the MBC was half of that of the latter. Thus, inclusion interaction did not affect the inhibitory and bactericidal effects of iodine against *E. coli* and *S. aureus*. Meanwhile, the different susceptibility of the iodine-loaded samples to the two bacteria mentioned above was due to the fact that iodine is more difficult to cross the cell wall of Gram-negative bacteria (38, 39).

I$_2$@nanocubes and I$_2$@microbars Reduced Levels of Pro-inflammatory Cytokines in MHS Cells

Since URT infections often cause a variety of inflammatory reactions, we checked LPS-induced expression of cytokines such as TNF-α, IL-1β, and IL-6 to investigate whether iodine-loaded carriers affected the production of pro-inflammatory mediators. Cytotoxicity of I$_2$@nanocubes and I$_2$@microbars was assessed using the MHS and A549 cells to evaluate the expression of cytokines at the cellular level. The cellular viability values of MHS and A549 cells were all more than 90% for the concentrations under 12.5 μg/mL of iodine, indicating minor toxicity (Fig. 5a, b). Based on the results of the cytotoxicity assays, the concentrations

(0.5, 2, and 10 μg/mL) of iodine were selected for inhibiting tests of pro-inflammatory cytokines. Our data showed that cells stimulated with LPS presented a large production of TNF-α, IL-1β and IL-6, while cells cultured with I$_2$@microbars or I$_2$@nanocubes at an iodine concentration of 10 μg/mL significantly reduced the production of TNF-α, IL-1β and IL-6 in MHS cells (Fig. 5c–e).

Irritation of I$_2$@microbars on Pharyngeal Tissue

The irritation of iodine was one of the major defects that limit its use (40). After analyzing the nasal and oral applications of PVP-I, Frank et al. (41) concluded that it was safe to use PVP-I in oral cavities at the concentration of 2.5% (0.25% available iodine). Therefore, 0.25% iodine-loaded sample in this study was used for the evaluation of pharyngeal irritation in rats. Evaluation indexes included pharyngeal and behavioral observations of rats, body weight changes, histopathological sections of the pharynx, and inflammatory factors. During the whole experimental period, all rats had normal drinking, feeding, and activity, and did not show any abnormalities such as mouth scratch or increase of oral secretion. Moreover, the body weight of rats (Fig. 6a) in the two dosing groups showed similar
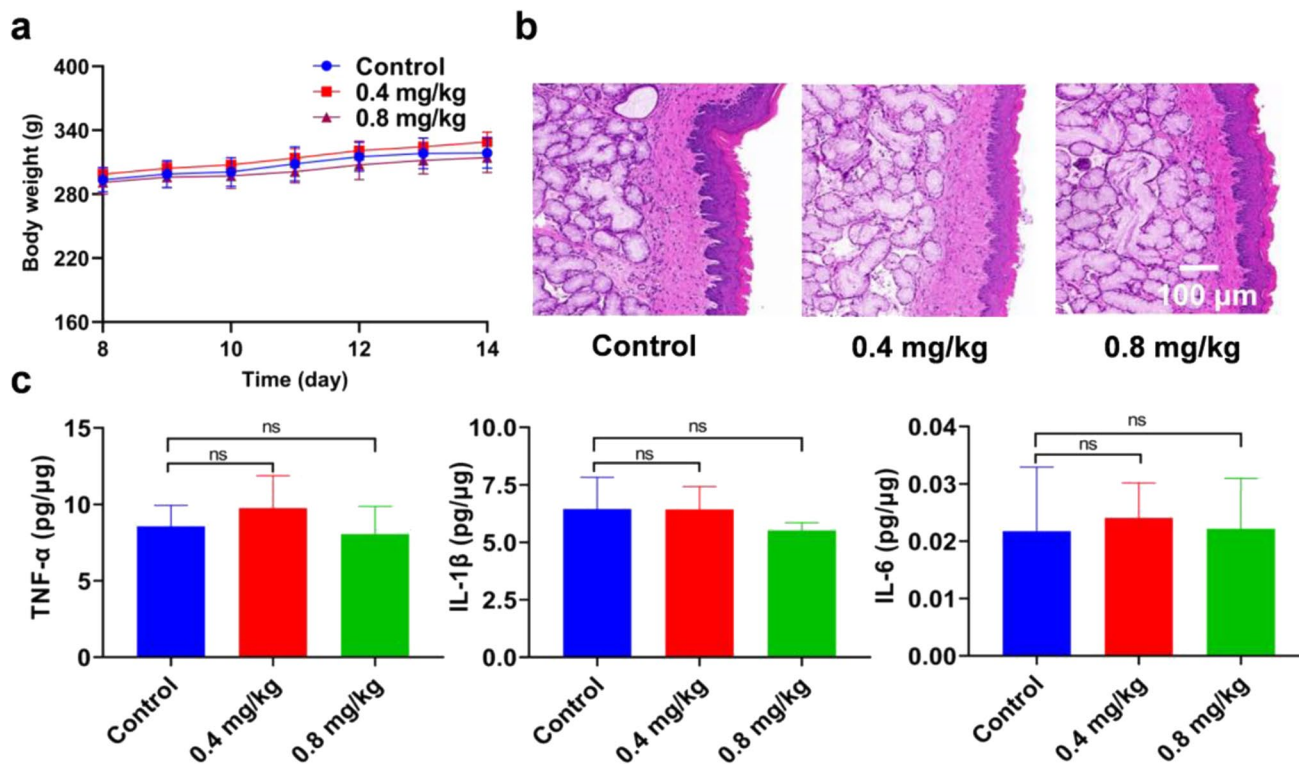
Fig. 6 Evaluation of pharyngeal irritation. **a** Body weight changes of rats. **b** H&E-stained slices of pharynx tissue from experimental rats. **c** The effects of I$_2$@microbars on TNF-α, IL-1β, and IL-6 levels in pharynx tissue of rats (ns, not significant)

increasing tendency as that in the blank group, and there was no significant difference between the three groups. In addition, no edema, congestion, bleeding, erosion, or ulceration of the pharynx was observed in the daily pharyngeal observations of the rats. The pathological changes of pharynx tissue were observed by H&E staining. As shown in Fig. 6b, the structural stratifications of the pharyngeal tissues of the control rats were clear, the mucosal epithelium was unkeratinized complex flat epithelium and did not show hyperplasia. Moreover, no inflammatory cell infiltration was found in the lamina propria. The glandular structure of the submucosa was normal; no vascular dilatation and bleeding were observed. There was no significant difference between the pharyngeal mucosa of the rats in the varied dose groups and the normal control rats. The inflammatory factor content of each rat's pharyngeal tissue was divided by its own total protein content to obtain the percentage share of inflammatory factors to eliminate individual variability. Data analysis showed no significant differences in the levels of inflammatory factors of the 0.4 mg/kg group or the 0.8 mg/kg group compared to the normal control group (Fig. 6c). The above results indicated that both doses of iodine-carrying microbars were not irritating to rat pharyngeal tissues under experimental conditions of continuous administration for 7 days, implying that I_2@microbars has great potential application for the treatment of URT infections.

CONCLUSION

In conclusion, KI-conjugated CD carriers were designed by controlled crystallization method and used for URT targeted drug delivery. Characterizations illustrated that the gas–solid reaction could efficiently encapsulate iodine into both the carriers. The evacuation rate of the powders was all above 98%, implying efficient drug release through the capsule containers. The microbars mainly deposited in the URT, while nanocubes were primarily delivered to the deep lungs. The aerodynamic properties of the iodine-loaded carriers did not change significantly at low drug loading, suggesting the potential to use the carriers for target delivery of drugs to a specific location in the respiratory tract. The results of antimicrobial, cellular, and animal experiments showed that the carriers have good biocompatibility and the iodine-loaded dry powders of I_2@microbars have antimicrobial effectiveness and low irritation on pharyngeal tissues. Overall, the present study provides novel treatment of URT infections via supramolecular cyclodextrin carriers for URT local therapy with iodine loading by a solvent-free method, which enhances the stability and reduces the inherent irritation without inhibiting their antimicrobial effects.

Author Contribution Kaikai Zhang, Xiaohong Ren, and Jiacai Chen contributed equally to this article. Kaikai Zhang carried out most experiments under the guidance of Jiwen Zhang, Li Wu, Weifeng Zhu, and Shujun Wang. Xiaohong Ren and Jiacai Chen helped to accomplish the antibacterial activity and cell experiments. Caifen Wang and Xiaojin Chen helped with the *in vitro* aerosol dispersion performance evaluation experiment. Siyu He, Ting Xiong, and Jiawen Su assisted with review. All authors discussed the results and commented on the manuscript.

Declarations

References

1. Murray CJL, Barber RM, Foreman KJ, Ozgoren AA, Abd-Allah F, Abera SF, et al. Global, regional, and national disability-adjusted life years (DALYs) for 306 diseases and injuries and healthy life expectancy (HALE) for 188 countries, 1990–2013: quantifying the epidemiological transition. Lancet. 2015;386(10009):2145–91.
2. Incze M, Grady D, Gupta A. I have a cold-what do I need to know? Jama Intern Med. 2018;178(9):1288.
3. Hasegawa K, Tsugawa Y, Cohen A, Camargo CA. Infectious disease-related emergency department visits among children in the US. Pediatr Infect Dis J. 2015;34(7):681–5.
4. Tiewsoh K, Kaur J, Lodha R, Kabra SK. Management of upper respiratory tract infection. Indian J Pediatr. 2008;75:S28–32.
5. Hur JK. Upper respiratory infections in children. J Korean Med Assoc. 2010;53(1):5–9.
6. Resch B, Kurath-Koller S, Eibisberger M, Zenz W. Prematurity and the burden of influenza and respiratory syncytial virus disease. World J Pediatr. 2016;12(1):8–18.
7. West JV. Acute upper airway infections. Br Med Bull. 2002;61:215–30.
8. Abdulah R. Antibiotic abuse in developing countries. Pharm Regul Aff. 2012;1:e106.
9. Mendelson M, Matsoso MP. The world health organization global action plan for antimicrobial resistance. Samj S Afr Med J. 2015;105(5):325.
10. Kelly SA, Rodgers AM, O'Brien SC, Donnelly RF, Gilmore BF. Gut check time: antibiotic delivery strategies to reduce antimicrobial resistance. Trends Biotechnol. 2020;38(4):447–62.
11. Jaume F, Valls-Mateus M, Mullol J. Common cold and acute rhinosinusitis: up-to-date management in 2020. Curr Allergy Asthma Rep. 2020;20(7):10.
12. Malesker MA, Callahan-Lyon P, Ireland B, Irwin RS, Panel CEC. Pharmacologic and nonpharmacologic treatment for acute

cough associated with the common cold CHEST expert panel report. Chest. 2017;152(5):1021–37.

13. Farhang B, Grondin L. The effect of zinc lozenge on postoperative sore throat: a prospective randomized, double-blinded, placebo-controlled study. Anesth Analg. 2018;126(1):78–83.

14. Pelletier JS, Tessema B, Frank S, Westover JB, Brown SM, Capriotti JA. Efficacy of povidone-iodine nasal and oral antiseptic preparations against severe acute respiratory syndrome-coronavirus 2 (SARS-CoV-2). Ent-Ear Nose Throat. 2021;100(2_SUPPL):192S-6S.

15. Eggers M, Koburger-Janssen T, Eickmann M, Zorn J. *In vitro* bactericidal and virucidal efficacy of povidone-iodine gargle/mouthwash against respiratory and oral tract pathogens. Infect Dis Ther. 2018;7(2):249–59.

16. Li X, Vogt FG, Hayes D, Mansour HM. Physicochemical characterization and aerosol dispersion performance of organic solution advanced spray-dried microparticulate/nanoparticulate antibiotic dry powders of tobramycin and azithromycin for pulmonary inhalation aerosol delivery. Eur J Pharm Sci. 2014;52:191–205.

17. Alabsi W, Acosta MF, Al-Obeidi FA, Hay M, Polt R, Mansour HM. Synthesis, physicochemical characterization, *in vitro* 2D/3D human cell culture, and *in vitro* aerosol dispersion performance of advanced spray dried and co-spray dried angiotensin (1–7) peptide and PNA5 with trehalose as microparticles/nanoparticles for targeted respiratory delivery as dry powder inhalers. Pharmaceutics. 2021;13(8):36.

18. Hu X, Wang C, Wang L, Liu Z, Wu L, Zhang G, et al. Nanoporous CD-MOF particles with uniform and inhalable size for pulmonary delivery of budesonide. Int J Pharm. 2019;564:153–61.

19. Lin Y, Wong J, Qu L, Chan H, Zhou Q. Powder production and particle engineering for dry powder inhaler formulations. Curr Pharm Des. 2015;21(27):3902–16.

20. Kou X, Chan LW, Sun CC, Heng PWS. Preparation of slab-shaped lactose carrier particles for dry powder inhalers by air jet milling. Asian J Pharm Sci. 2017;12(1):59–65.

21. Labiris NR, Dolovich MB. Pulmonary drug delivery. Part I: physiological factors affecting therapeutic effectiveness of aerosolized medications. Br J Clin Pharmacol. 2003;56(6):588–99.

22. Gradon L, Sosnowski TR. Formation of particles for dry powder inhalers. Adv Powder Technol. 2014;25(1):43–55.

23. Kadota K, Sosnowski TR, Tobita S, Tachibana I, Tse JY, Uchiyama H, et al. A particle technology approach toward designing dry-powder inhaler formulations for personalized medicine in respiratory diseases. Adv Powder Technol. 2020;31(1):219–26.

24. Durani P, Leaper D. Povidone-iodine: use in hand disinfection, skin preparation and antiseptic irrigation. Int Wound J. 2008;5(3):376–87.

25. Eggers M. Infectious disease management and control with povidone iodine. Infect Dis Ther. 2019;8(4):581–93.

26. Gershenfeld L. Iodine as a virucidal agent. J Pharm Sci. 2010;44(3):177–82.

27. Khan MM, Parab SR. Tolerability and usability of 0.5% PVP-I gargles and nasal drops in 6692 patients: observational study. Am J Otolaryngol. 2021;42(2):4.

28. Abdelkader H, Fathalla Z, Moharram H, Ali TF, Pierscionek B. Cyclodextrin enhances corneal tolerability and reduces ocular toxicity caused by diclofenac. Oxid Med Cell Longev. 2018;2018:1–13.

29. Jansook P, Kulsirachote P, Loftsson T. Cyclodextrin solubilization of celecoxib: solid and solution state characterization. J Incl Phenom Macro. 2018;90(1):75–88.

30. Gadade DD, Pekamwar SS. Cyclodextrin based nanoparticles for drug delivery and theranostics. Adv Pharm Bull. 2020;10(2):166–83.

31. Rao MRP, Chaudhari J, Trotta F, Caldera F. Investigation of cyclodextrin-based nanosponges for solubility and bioavailability enhancement of rilpivirine. AAPS Pharm Sci Tech. 2018;19(5):2358–69.

32. Ohtani Y, Irie T, Uekama K, Fukunaga K, Pitha J. Differential effects of α-, β- and γ-cyclodextrins on human erythrocytes. Eur J Biochem. 1989;186(1–2):17–22.

33. Marui Y, Kida T, Akashi M. Facile morphological control of cyclodextrin nano- and microstructures and their unique organogelation ability. Chem Mat. 2010;22(2):282–4.

34. Lu S, Ren X, Guo T, Cao Z, Sun H, Wang C, et al. Controlled release of iodine from cross-linked cyclodextrin metal-organic frameworks for prolonged periodontal pocket therapy. Carbohydr Polym. 2021;267:11.

35. Zhao K, Guo T, Wang C, Zhou Y, Xiong T, Wu L, et al. Glycoside scutellarin enhanced CD-MOF anchoring for laryngeal delivery. Acta Pharm Sin B. 2020;10(9):1709–18.

36. Lu X, Chen L, Wu C, Chan H, Freeman T. The effects of relative humidity on the flowability and dispersion performance of lactose mixtures. Materials. 2017;10(6):9.

37. Lebrun P, Krier F, Mantanus J, Grohganz H, Yang MS, Rozet E, et al. Design space approach in the optimization of the spray-drying process. Eur J Pharm Biopharm. 2012;80(1):226–34.

38. Xu N, Ding D. Preparation and antibacterial activity of chitosan derivative membrane complexation with iodine. RSC Adv. 2015;5(97):79820–8.

39. Au-Duong A-N, Lee C-K. Iodine-loaded metal organic framework as growth-triggered antimicrobial agent. Mater Sci Eng C Mater Biol Appl. 2017;76:477–82.

40. Borrego L, Hernandez N, Hernandez Z, Penate Y. Povidone-iodine induced post-surgical irritant contact dermatitis localized outside of the surgical incision area. Report of 27 cases and a literature review. Int J Dermatol. 2016;55(5):540–5.

41. Frank S, Capriotti J, Brown SM, Tessema B. Povidone-iodine use in sinonasal and oral cavities: a review of safety in the COVID-19 era. Ent-Ear Nose Throat. 2020;99(9):586–93.